Effect of Sample Heterogeneity on the Interpretation of QCM(−D) Data: Comparison of Combined Quartz Crystal Microbalance/Atomic Force Microscopy Measurements with Finite Element Me...

ARTICLE *in* ANALYTICAL CHEMISTRY · NOVEMBER 2008

Impact Factor: 5.64 · DOI: 10.1021/ac8013115 · Source: PubMed

4 AUTHORS, INCLUDING:

Ilya Reviakine
Karlsruhe Institute of Technology
52 PUBLICATIONS **2,149** CITATIONS
SEE PROFILE

Elena Rojas
CIC biomaGUNE
17 PUBLICATIONS **214** CITATIONS
SEE PROFILE

Effect of Sample Heterogeneity on the Interpretation of QCM(-D) Data: Comparison of Combined Quartz Crystal Microbalance/Atomic Force Microscopy Measurements with Finite Element Method Modeling

Diethelm Johannsmann,*,† Ilya Reviakine,*,‡ Elena Rojas,‡ and Marta Gallego‡

Institute of Physical Chemistry, Clausthal University of Technology, Clausthal-Zellerfeld, D-38678, Germany, and Centro de Investigacion Cooperativa en Biomateriales, Parque Tecnológico de San Sebastián, E-20009 San Sebastián, Spain

A quartz crystal microbalance was integrated into an AFM in order to monitor the adsorption of biomolecules to the resonator surface with both atomic force microscopy and microgravimetry. The comparison between the two techniques allows the fractional coverage of the surface, θ, to be correlated with the frequency shift of the resonator, Δf. The adsorbed material was ferritin, which is a spherical protein with a diameter of ~12 nm. Even at a coverage below 50%, the protein layer exhibits Sauerbrey-like behavior, meaning that the magnitude in the frequency shift $|\Delta f|$ much exceeds the shift in bandwidth and that the normalized frequency shift, $\Delta f/n$ (n the overtone order), is similar on the different overtones. The relation between coverage and frequency shift was found to be nonlinear. In order to model this situation, we performed finite element method calculations based on the incompressible Navier−Stokes equation. The comparison between the model and the experiment suggests that the deformation of the protein upon adsorption is small. For low coverage, the volume of the trapped solvent exceeds the volume of the adsorbate itself. The ratio of the two decreases with increasing coverage. This is the cause of the experimentally observed nonlinear relationship between the surface coverage and frequency shift. Comparing frequency shifts at different overtones, one finds that $\Delta f/n$ slightly decreases with overtone order. Such a behavior is typically attributed to softness. The model shows that, for the adsorbed spheres, this apparent softness arises through a rocking motion of the spheres at the surface instead of the shear deformation. Also, there is a hydrodynamic contribution (related to roughness) to the overtone dependence of $\Delta f/n$.

In the past years, the quartz crystal microbalance (QCM) has seen an impressive broadening of uses.[1] Its potential applications go much beyond microgravimetry.[2] Acoustic sensing of viscosity is now routine.[3,4] Effects of viscoelasticity are well understood for planar layer systems.[5−9] As the samples have become more and more complex, lateral heterogeneity has turned into one of the biggest hurdles in quantitative modeling. Many biologically motivated investigations concern adsorbed objects, which are spatially separated. Examples are vesicles,[10,11] proteins,[12,13] viruses,[14] or DNA strands.[15,16] More generally, adsorption often proceeds such that the coverage is inhomogeneous at intermediate times, even if the final adsorbate forms a smooth film. Such samples, a priori, cannot be treated as if they were homogeneous films.

While modeling of heterogeneous samples might appear to be demanding, the general approach is rather clear, when basing the analysis on the small-load approximation (see eq 1 below). On a fundamental level, the frequency shift, Δf, is proportional to the ratio of (average) stress and speed at the resonator surface.[1,5] The well-known formalism of QCM data analysis for planar layer systems (including the Sauerbrey equation[17] and the Gordon-Kanazawa result[3,4]) follows straightforwardly from the small-load approximation, if the stress is calculated with theory of planar acoustic multilayers. Before elaborating on the extension of the

* To whom correspondence should be addressed. E-mail: johannsmann@pc.tu-clausthal.de; ireviakine@cicbiomagune.es.

† Clausthal University of Technology.

‡ Parque Tecnológico de San Sebastián.

(1) Steinem, C., Janshoff, A., Eds. *Piezoelectric Sensors*; Springer: New York, 2006.
(2) Lu, C., Czanderna, A. W., Eds. *Applications of Piezoelectric Quartz Crystal Microbalances*; Elsevier: Amsterdam, 1984.
(3) Borovikov, A. P. *Instrum. Exp. Techn.* **1976**, *19*, 223.
(4) Kanazawa, K. K.; Gordon, J. G., II *Anal. Chim. Acta* **1985**, *99*, 175.
(5) Johannsmann, D. *Macromol. Chem. Phys.* **1999**, *200*, 501;. eq 13.
(6) Nakamoto, T.; Moriizumi, T. *Jpn. J. Appl. Phys.* **1990**, *29*, 963.
(7) Bandey, H. L.; Martin, S. J.; Cernosek, R. W.; Hillman, A. R. *Anal. Chem.* **1999**, *71*, 2205.
(8) Lucklum, R.; Behling, C.; Hauptmann, P. *Anal. Chem.* **1999**, *71*, 2488.
(9) Benes, E. *J. Appl. Phys.* **1984**, *56*, 608.
(10) Keller, C. A.; Kasemo, B. *Biophys. J.* **1998**, *75*, 1397.
(11) Reimhult, E.; Hook, F.; Kasemo, B. *Langmuir* **2003**, *19*, 1681.
(12) Hook, F.; Rodahl, M.; Brzezinski, P.; Kasemo, B. *J. Colloid Interface Sci.* **1998**, *208*, 63.
(13) Hemmersam, A. G.; Rechendorff, K.; Besenbacher, F.; Kasemo, B.; Sutherland, D. S. *J. Phys. Chem. C* **2008**, *112*, 4180.
(14) Cooper, M. A.; Dultsev, F. N.; Minson, T.; Ostanin, V. P.; Abell, C.; Klenerman, D. *Nat. Biotechnol.* **2001**, *19*, 833.
(15) Larsson, C.; Rodahl, M.; Hook, F. *Anal. Chem.* **2003**, *75*, 5080.
(16) Tsortos, A.; Papadakis, G.; Mitsakakis, K.; Melzak, K. A.; Gizeli, E. *Biophys. J.* **2008**, *94*, 2706.
(17) Sauerbrey, G. *Z. Phys.* **1959**, *155*, 206.

10.1021/ac8013115 CCC: $40.75 © XXXX American Chemical Society
Published on Web 10/28/2008

formalism to heterogeneous loads, we comment on the existing approaches dealing with heterogeneity.

Laterally heterogeneous samples can be dealt with on an analytical basis if the scale of heterogeneity is much larger than the wavelength of sound, λ. The former case has been investigated by Flanigan and co-workers.[18] These authors studied the contact between a hemispherical cap of a soft polymer and a resonator. The radius of contact was much larger than λ.[18] Inside the contact area, the interaction between the resonator and the sample was assumed to be the same as for the semi-infinite viscoelastic medium. However, the contact area was smaller than the active area of the crystal. It turns out that the effect of the finite contact area can be accounted for by a prefactor, which is the ratio of the contact area and the resonator's active area. This formalism works well both in air and in liquids. There also is a formalism covering the opposite limit of "point contacts", that is, well separated contacts, the size of which is much smaller than λ.[19,20] This theory works well for dry granular media or multicontact interfaces in air.[21]

Heterogeneity also is unproblematic for Sauerbrey films in air. These films are much thinner than λ. For such samples, the Sauerbrey equation may be applied in an average sense. Δf is proportional to the average mass per unit area at the crystal surface.[22]

In liquids, to the contrary, heterogeneous samples pose problems even if they are very thin. Predicting the mean stress at the resonator surface is a tough problem for all but the simplest geometries. Complications arise, because the adsorbed objects interact via hydrodynamics. Hydrodynamic interactions are long-ranged, and one may not treat an assembly of adsorbed objects as isolated objects. (This approximation is permitted in air.) Consider, for example, two spheres adsorbed in near proximity. The water contained in the gap will to some (unknown) extent be dragged along by the spheres in their movement. The liquid will therefore act is if it were part of the adsorbed mass and the "Sauerbrey mass" will contain a contribution from trapped solvent. This problem is of paramount importance in the quantitative interpretation of QCM data.

Even though predicting Δf for heterogeneous loads in liquids is difficult, there is an analytical solution for a particular type of geometry.[23] This solution applies to shallow sinusoidal corrugation waves on the crystal surface. The mathematical effort is considerable. Once the solution for a single wave with wave-vector q has been obtained, one can decompose arbitrary rough surfaces into their Fourier components, and add up all contributions in order to obtain the shifts of frequency and bandwidth. Again, this approach requires that the vertical scale of roughness be much less than the wavelength of sound (or, in the language of ref 23, the depth of penetration, δ).

On a pragmatic level, most researchers have in the past treated heterogeneous layers as effectively homogeneous. Parameters describing the layer (its thickness and the complex shear modulus, G_f, or its inverse, J_f) obtained from fitting experimental data with such models implicitly account for hydrodynamic effects in one way or another. Effective medium theories are time-honored and have certainly been successful in many fields of science. They are an established practice in optics, where a dilute adsorbate often is treated as a continuous film with a suitably lowered refractive index. A similar approach is taken in rheology, where dispersions of solid particles are treated as a homogeneous liquid with an effective, macroscopic viscosity different from the solvent viscosity.[24] In passing, we note that the effective medium theories are more problematic in acoustics than in optics for the reasons discussed in ref 25. Interestingly, there is an effective medium theory of rough adsorbates that explicitly addresses hydrodynamics effects.[26,27] The adsorbate is treated as a porous medium, where the flow of the liquid through the medium is described by the Brinkman equation. The model contains a "permeability parameter", ξ, describing the openness of the equivalent medium. We will come back to this model in the results section.

The investigation reported here concerns a geometry (namely, adsorbed spheres of nanometer dimension), which at this time is not amenable to a rigorous analytical description. Rather than simplifying the situation to the extent that analytical equations would cover it, we resort to numerical modeling.

On the experimental side, shifts of frequency and bandwidth were acquired as a function of coverage for a model substance, which was the protein ferritin.[28] Ferritin is an iron storage protein consisting of a protein shell (apoferritin) and an iron core. In solution, ferritin molecules are nearly spherical, with a diameter of ~12 nm. Both forms (ferritin and apoferritin) have been thoroughly investigated with respect to their adsorption at surfaces[12,29,13,30,31] and intermolecular interactions[32−34] and are offering promise in the developing field of bionanotechnology.[35] Quartz crystals were mounted on an atomic force microscope (AFM).[36−38] This allowed the ferritin coverage at the crystal surface to be determined by AFM in parallel to the QCM measurements, in situ and in liquid (Figure 1). On the side of modeling, we employed the finite element method (FEM). The assumptions entering the modeling are very limited. The modeling results match the experimental data well (Figure 2).

(18) Flanigan, C. M.; Desai, M.; Shull, K. R. *Langmuir* **2000**, *16*, 9825.
(19) Laschitsch, A.; Johannsmann, D. *J. Appl. Phys.* **1999**, *85*, 3759.
(20) Dybwad, G. L. *J. Appl. Phys.* **1985**, *58*, 2789.
(21) D'Amour, J. N.; Stålgren, J. J. R.; Kanazawa, K. K.; Frank, C. W.; Rodahl, M.; Johannsmann, D. *Phys. Rev. Lett.* **2006**, *96*, 058301.
(22) Averaging needs to account for the variable amplitude of oscillation ("energy trapping") with a suitable statistical weight.
(23) Urbakh, M.; Daikhin, L. *Phys. Rev. B* **1994**, *49*, 4866.
(24) Hunter, R. J. *Foundations of Colloid Science*; Oxford University Press: New York, 2005.
(25) Plunkett, M. A.; Wang, Z.; Rutland, M. W.; Johannsmann, D. *Langmuir* **2003**, *19*, 6837.
(26) Daikhin, L.; Gileadi, E.; Katz, G.; Tsionsky, V.; Urbakh, M. *Anal. Chem.* **2002**, *74*, 554.
(27) Bund, A.; Schneider, M. *J. Electrochem. Soc.* **2002**, *149*, E331.
(28) Granick, S. *Chem. Rev.* **1946**, *38*, 379.
(29) Johnson, C. A.; Yuan, Y.; Lenhoff, A. M. *J. Colloid Interface Sci.* **2000**, *223*, 261.
(30) Caruso, F.; Furlong, D. N.; Kingshott, P. *J. Colloid Interface Sci.* **1997**, *186*, 129.
(31) Lavalle, P.; Gergely, C.; Lustig, A.; Ball, V. *J. Chem. Phys.* **2000**, *113*, 8212.
(32) Yau, S. T.; Thomas, B. R.; Vekilov, P. G. *Phys. Rev. Lett.* **2000**, *85*, 353.
(33) Thomas, B. R.; Carter, D. *J. Cryst. Growth* **1998**, *187*, 499.
(34) Petsev, D. N.; Thomas, B. R.; Yau, S. T.; Vekilov, P. G. *Biophys. J.* **2000**, *78*, 2060.
(35) Kumagai, S.; Yoshii, S.; Yamada, K.; Matsukawa, N.; Fujiwara, I.; Iwahori, K.; Yamashita, I. *Appl. Phys. Lett.* **2006**, *88*, 153103.
(36) Hayden, O.; Bindeus, R.; Dickert, F. L. *Meas. Sci. Technol.* **2003**, *14*, 1876.
(37) Friedt, J. M.; Choi, K. H.; Frederix, F.; Campitelli, A. *J. Electrochem. Soc.* **2003**, *150* (10), H229-H234.
(38) Bund, A.; Schneider, O.; Dehnke, V. *Phys. Chem. Chem. Phys.* **2002**, *4*, 3552.

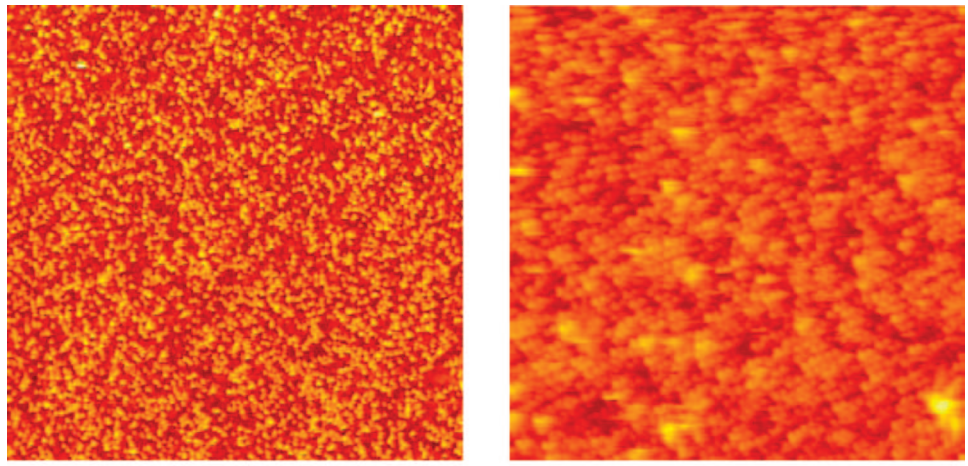

Figure 1. AFM images of ferritin monomers adsorbed on the surface of the gold electrodes covering the quartz crystals. The resonator was integrated into an AFM. The coverage was derived from counts of the number of adsorbed spheres and used as the ordinate in plots of QCM frequency and bandwidth shifts in Figure 2a. The images are 5 × 5 μm^2 and 1 × 1 μm^2, respectively. The vertical scale in both cases is 50 nm. The ferritin packing densities (surface coverages) corresponding to these particular two images were 4% and 30%.

EXPERIMENTAL SECTION

Details of sample preparation and the experimental setup are described in a separate publication.[39] Crucial for the success of these experiments were ferritin purification and cleaning of the QCM crystal surfaces. Briefly, a commercial equine spleen ferritin stock solution (Sigma-Aldrich, Madrid, Spain) was purified by size exclusion chromatography to separate dimers and higher-order aggregates from the monomers. The purity of the monomers was established by electron microscopy and dynamic light scattering. The monomer fraction was used in all experiments described here; the effect of impurities on the QCM response is discussed in ref 39. The 5-MHz quartz crystals with evaporated gold electrodes were purchased from Q-Sense (Gothenburg, Sweden). They were cleaned overnight in 2% SDS solution (Sigma-Aldrich, Madrid, Spain), rinsed with Nanopure water, and cleaned in a mixture of ammonium hydroxide and hydrogen peroxide (1:1:1.5 with water; chemicals were purchased from Scharlab, Barcelona, Spain) at 80 °C for 10 min, rinsed once more with Nanopure water, and cleaned in air plasma for 12 min in a PDC-002 plasma cleaner set at "high" (30 W). After cleaning, the crystals were used immediately. After each experiment, the crystals were cleaned in 2% SDS solution overnight and rinsed with copious amounts of water. It was quite critical for the success of the experiments not to let the protein dry on the surface. Ferritin monomers were adsorbed to the cleaned resonator surface (gold) from buffer solutions of varying protein and salt concentrations to achieve various surface coverage.

Figure 1 shows typical AFM images obtained in the AFM-QCM setup. A quartz crystal was mounted in a special homemade holder on the variable-temperature stage of a Veeco Multimode atomic force microscope connected to a Nanoscope V controller (Veeco, Instruments, Santa Barbara, CA). The crystal was connected to a SA250C network analyzer (Saunders, AZ) and controlled by the software package QTZ (Resonant Probes GmbH, Goslar, Germany). AFM images were collected in tapping mode. Oxide-sharpened silicon nitride tips mounted on V-shaped cantilevers with a nominal spring constant of 0.32 N/m were used to obtain the images. The ferritin surface coverage was determined by counting the number of particles in a given area. Figure 2 shows the shifts of frequency, Δf, and damping, $\Delta\Gamma$ (where Γ is the half-bandwidth at half-maximum), versus the coverage thus derived.

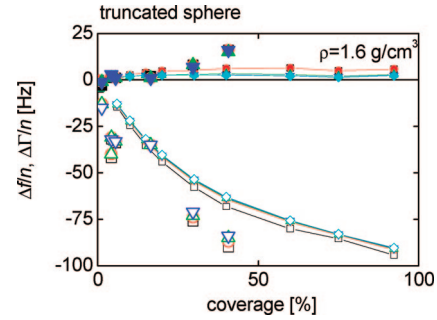

Figure 2. Shifts of frequency and bandwidth versus coverage. Large symbols: experimental values. Small symbols with lines: results from FEM modeling with truncated cylinders. The FEM results are arithmetic means of the results obtained with the flow direction perpendicular and along the cylinders.

Modeling. FEM calculations were employed, using the Multiphysics Module of the COMSOL software package (COMSOL GmbH, Göttingen, Germany). The calculation of the frequency shift, Δf, builds on the small-load approximation, which states that Δf is proportional to the stress/speed ratio at the crystal surface[40,41]

$$\frac{\Delta f^*}{f_F} \approx \frac{i}{\pi}\frac{Z_L}{Z_q} = \frac{i}{\pi Z_q}\frac{\sigma}{\dot{u}} \qquad (1)$$

Here $\Delta f^* = \Delta f + i\Delta\Gamma$ is the complex frequency shift, f_F is the frequency of the fundamental, $Z_q = 8.8 \times 10^6$ kg m^{-2} s^{-1} is the

(39) Rojas, E.; Gallego, M.; Reviakine, I. *Anal. Chem.*, in press.

(40) Eggers, F.; Funck, Th. *J. Phys. E: Sci. Instrum.* **1987**, *20*, 523.

(41) Johannsmann, D.; Mathauer, K.; Wegner, G.; Knoll, W. *Phys. Rev. B* **1992**, *46*, 7808.

acoustic impedance of AT-cut quartz, Z_L is the load impedance, σ is the tangential stress, and $\dot{u}$ is the lateral speed at the resonator surface. The load impedance is the acoustic analog of the electrical impedance, where the latter is a voltage/current ratio, rather than a stress/speed ratio. Equation 1 holds in a very general sense. Both the Sauerbrey equation[17] and the Gordon-Kanazawa result[3,4] are derived from eq 1 by inserting the respective stress/speed ratios. For instance, the stress at the bottom of a thin film in air is mostly caused by inertia. It is given by $\sigma = m_f \partial^2 u/\partial t^2 = -\omega^2 m_f u$ (with m_f the mass per unit area and u the amplitude of lateral displacement) $\dot{u}$ is equal to $i\omega u$. Inserting these relations into eq 1, one straightforwardly recovers the Sauerbrey equation.

Since the frequency shift depends linearly on stress, the small-load approximation holds in an average sense. For heterogeneous samples (such as adsorbed proteins or vesicles) one may insert the area-average of the stress distribution into eq 1. Even for complicated geometries, this average stress can be computed numerically. In this way, the small-load approximation opens the way to study structured materials with the QCM. The small-load approximation is an essential concept, since it relates shifts of frequency and bandwidth, on the one hand, with the stress pattern at the boundary between the resonators and a complex sample, on the other.

Within the small-load approximation, it is a priori not possible to distinguish between inertial loading (also termed "mass loading"), viscous loading, elastic loading, or other types of interactions. For structured samples, there are no clear-cut distinctions between these different loads. Inertia, elasticity, and viscosity all play some role, but any given average stress cannot be decomposed into contributions from inertia, viscosity, and elasticity. Also, one may not just relate Δf to mass and $\Delta\Gamma$ to viscosity.

Equation 1 has the tangential stress on the right-hand side. Ignoring the normal stress components is justified in the Appendix. The appendix derives a more general form the small-load approximation. This form applies to arbitrary resonators and arbitrary loads.

We employed the FEM to compute the distribution of tangential stress for the specific geometry under consideration here (truncated spheres). Technical details and some steps of validation of the FEM calculations are provided in the Supporting Information. In the following, we discuss some assumptions and the range of applicability.

Our computational resources only allowed for two-dimensional FEM calculations. 3D modeling is possible, in principle, but one cannot afford the appropriate mesh size on a personal computer. We approximated the adsorbate as a truncated sphere, where a "sphere" turns into a cylinder, in 2D. For every geometry, we performed two calculations, where the direction of flow was either parallel or perpendicular to the cylinders. When making the comparison with experiment, we used the arithmetic averages of Δf and $\Delta\Gamma$ as determined for the two directions of flow.

We modeled the ferritin molecule as a sphere of diameter 12 nm, which is consistent with the AFM images (Figure 1) and the literature.[42] The spheres were modeled as continuous media without internal structure. Molecular details are not covered. For most calculations, the compression of the sphere at the point of contact was 1 nm. For comparison, we also investigated adsorbed hemispheres of the same volume (that is, truncated spheres, where the compression amounted to 50% of the diameter). Figure 3 shows the geometries and the meshes employed. Periodic boundaries were applied at the top and the bottom. The geometry therefore corresponds to an array of cylinders rather than an individual cylinder. Figure 4 displays contour plots of a typical solution. Panels a–c concern flow perpendicular to the cylinders. Panels a and b show contour plots of the speed of flow along the vertical and the horizontal, respectively. "+" and "−" indicate flow to the right and to the left. Panel c displays the pressure. Note the strong peaks of pressure close to the three-phase line. Panel d concerns flow parallel to the cylinders (that is, perpendicular to the plane of the paper). For the latter geometry, both the orthogonal component of the speed and the pressure vanish identically. The density of the spheres was chosen as $\rho = 1.6$ g/cm^3. In the experiment, ρ depends on the loading with iron.

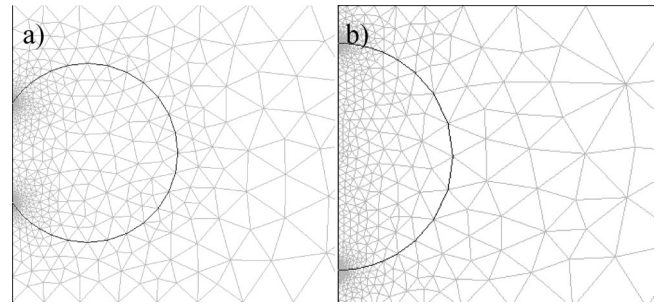

Figure 3. Employed geometries and meshing. The height of the cells displayed here was 20 nm, corresponding to a nominal coverage of 60%. The nominal coverage here is the ratio of the sphere diameter in the undistorted state (12 nm) and the height of the cell. The cell height was varied in order to emulate variable coverage. The cell has been cut off on the right-hand side for clarity. It extends to $z = 2\ \mu$m, which is well beyond the penetration depth δ (252 nm at $f = 5$ MHz).

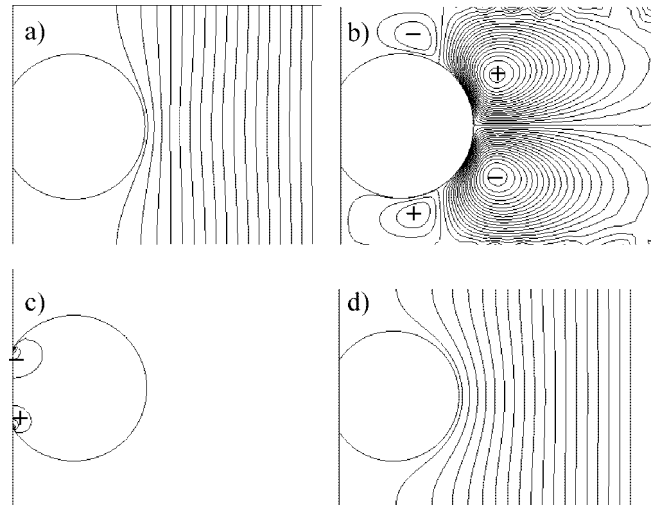

Figure 4. Modeling results for the geometry shown in Figure 3a. Panels a–c show results for a flow perpendicular to the axis of the cylinder. (a, vertical component of the speed; b, horizontal component of speed; c, pressure). Panel d shows the speed for a geometry, where the direction of flow is along the cylinders. In this case, the model just contains one component of the speed. Both the pressure and the orthogonal component of the speed vanish identically. "+" and "−" denote positive and negative values.

(42) Massover, W. H. *Micron* **1993**, *24*, 389.

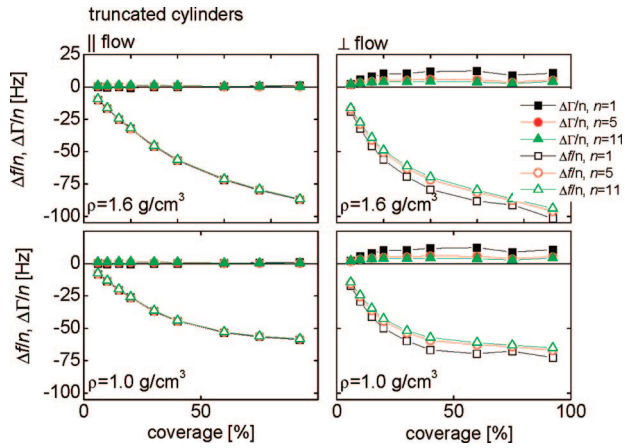

Figure 5. Shifts of frequency and bandwidth versus coverage for truncated cylinders (Figure 3a).

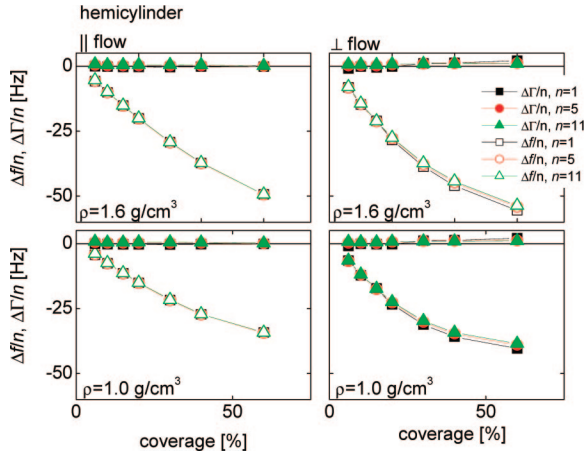

Figure 6. Shifts of frequency and bandwidth versus coverage for hemicylinders (Figure 3b).

Incomplete loading (which is possible) would result in a somewhat lower density. For this reason, calculations were also performed with $\rho = 1.0$ g/cm^3, which would correspond to the unloaded case.

Comparison of Figure 4a and d (flow perpendicular and parallel to the cylinders) shows that that solvent trapping is more efficient for perpendicular flow. The solvent in-between neighboring particles moves at a higher speed for perpendicular flow. In the cases of perpendicular flow, trapping is accomplished by both viscous coupling and pressure gradients, while there are no pressure gradients ($p \equiv 0$) for parallel flow. Still, there is some solvent trapping, in the latter case as well. The fact that trapping is more efficient for perpendicular flow is also reflected in the frequency versus coverage curves displayed in Figures 5 and 6. The nonlinearity is stronger for perpendicular flow.

A significant assumption concerns stiffness. At this point, we focus on effects of hydrodynamics, staying away from viscoelasticity. As explained in detail in the results section, the spheres must be almost glassy (stiffness in the range of 1 GPa) in order not to show viscoelastic effects. In reality, ferritin presumably is less rigid, and this will have to be accounted for in more accurate future models.

The model at this point does not have adaptive meshing. The sphere surface did not deform. The sphere is a "subdomain" with certain material parameters. We prove in the Supporting Information that this shortcoming does not affect the frequency shifts in the small-amplitude limit. The amplitude of oscillation used in the FEM modeling was 0.01 nm.

RESULTS AND DISCUSSION

Figures 5 and 6 show the output of the modeling in terms of Δf and $\Delta\Gamma$. Shifts of frequency and bandwidth are displayed versus coverage. There are two geometries (truncated cylinder and hemicylinder), two directions of flow (parallel and perpendicular), and two densities (1.6 and 1.0 g/cm^3, corresponding to the iron-loaded and the unloaded protein). "Coverage" was the ratio of 12 nm (diameter of undeformed ferritin) and the height of the simulation cell.

The agreement with the experimental data (Figure 2) is quite impressive, given that there was not much freedom with regard to the input to the modeling. As shown in the Supporting Information, the FEM model also reproduces the analytical results from ref 23 for surfaces with shallow roughness. These findings lend credibility to the technique, as such.

In accordance with experiment, $\Delta\Gamma$ is much smaller than $|\Delta f|$. Also, the overtone dependence of the normalized frequency shift, $\Delta f/n$, is small. From the experimental side, the layer appears almost like a Sauerbrey film. Converting the frequency shift at full coverage to an equivalent Sauerbrey thickness, one finds a value close to the diameter of the sphere (12 nm). The fact that the truncated spheres with a compression of 1 nm match the experimental results much better than the hemispheres does not come as a surprise. Ferritin is not expected to flatten out at the surface. The AFM micrographs give no evidence of a large deformation.

In experimental studies, it is common to convert frequency shift to adsorbed amount, assuming a linear relationship between the two. Our results clearly display a nonlinearity. There is saturation at high coverage. The saturation is weaker for the higher density because of the mismatch in density between the adsorbate and the solvent. This finding is very important for quantitative analysis of QCM data. It shows that Δf is not proportional to coverage.

It is instructive to vary the density of the spheres, ρ, for a fixed geometry (Figure 7). Within the numerical accuracy, Δf and the density of the adsorbed object are linearly related. That entails the possibility of calculating the amount of trapped solvent. Solvent molecules taking part in the motion of the adsorbate for hydrodynamic reasons are known to contribute to the Sauerbrey mass, but how much solvent, exactly, is contained in the Sauerbrey mass for any given geometry is not usually known. For the simulation, the solvent's contribution to the Sauerbrey mass corresponds to the intercept of the Δf versus ρ-plot. For instance, this intercept is -31 Hz for the case displayed in Figure 7c. In Figure 7d, we went one step further and determined the contribution of the solvent for different coverages. One can straightforwardly divide the solvent's contribution to Δf by the contribution of the spheres. This quantity has been termed "fractional trapped solvent" in Figure 7. The fractional trapped solvent can exceed unity because it is normalized to the contribution of the spheres (as opposed to the total frequency shift). Not surprisingly, the fractional trapped solvent decreases with coverage.[43] Also, it is larger for perpen-

(43) A similar result has recently been obtained based on the comparison between optical and acoustic thickness, Richter, R. P. Private communication.

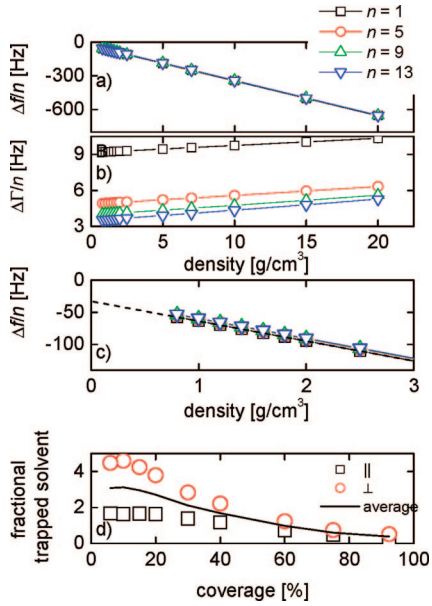

Figure 7. Shifts of frequency (a) and bandwidth (b) versus density for the truncated sphere. The coverage was 60%, the flow direction was perpendicular to the cylinder. A strictly linear relation was found for all other geometries and flow directions, as well. It is consequence of the fact the viscoelasticity is insignificant. Even though the layer is rough, it behaves essentially like a Sauerbrey film. Panel c shows an enlargement of panel a. The intercept of $\Delta f(\rho)$ with the *y*-axis is the contribution of the trapped solvent to the Sauerbrey mass. Panel d shows the contribution of solvent to the Sauerbrey mass (see text).

dicular flow than for flow along the direction of the cylinder. Considering the dilute limit and averaging over the two orientations of flow, one finds the trapped solvent to be about three times as large as the volume of the adsorbate itself. At a coverage of ~50%, this contribution comes out to be ~1.8. This compares well with the value of 1.73 that is expected from the volume of solvent trapped by a random-close-packed assembly of spheres.[44] A close value was also experimentally observed in ref 45.

The focus of this work was on roughness and hydrodynamics. To this end, the spheres were modeled as "rigid". We assigned a (high) complex viscosity ($\eta = \eta' - i\eta''$) to the spheres. More details on soft spheres are provided in the Supporting Information. The modulus of the viscosity ($\eta^* = (\eta'^2 + \eta''^2)^{1/2}$) was chosen high enough to ensure that neither Δf nor $\Delta\Gamma$ depended on the loss angle or on the exact value of η^*. As shown in Figure 8, this occurred when η^* was ~10^5 times the viscosity of water η_{wat}. This value was used in the calculations leading to the data displayed in Figures 2, 5, 6, and 7. The ratio of η' to η'' (the loss tangent) was chosen as 0.16. Again, the major part of the calculations was carried out with spheres that were essentially rigid. The finite (but very high) modulus was chosen for reasons of computational convenience and compatibility with those calculations, where the spheres actually were not rigid (see Figure 8a). Choosing rigid objects is meant to be a start. Presumably, ferritin molecules are

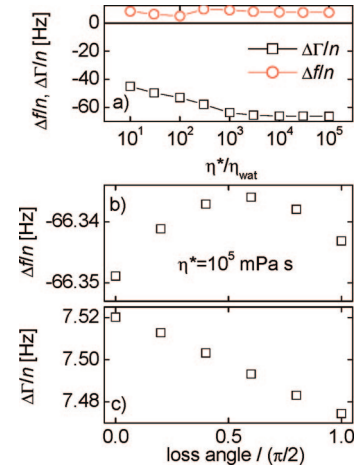

Figure 8. Shifts of frequency and bandwidth versus viscosity. η^* is defined as $\eta^* = (\eta'^2 + \eta''^2)^{1/2}$, where η' and η'' are the real and the imaginary parts of the viscosity. The loss angle, δ_L is defined via $\tan(\delta_L) = \eta'/\eta''$. The simulation results do not depend on the sphere's viscoelastic properties as long as η^* is above 10^4 m Pa s. The sphere can be considered as perfectly rigid. The loss tangent is unessential, as well. All simulations were carried out at $\eta^* = 10^5$ m Pa s. At a frequency of 5 MHz, a value of $\eta^* = 10^5$ m Pa s corresponds to a shear modulus of $G^* = |i\omega\eta^*| = 0.3$ GPa.

not rigid in the sense discussed above. It is even doubtful that a shear modulus (a macroscopic parameter) may be assigned to ferritin molecules in a meaningful way. Further studies are needed to account for finite stiffness.

The fact that η^*/η_{wat} had to be so high (~10^5) in order to avoid viscoelastic effects, came as somewhat of a surprise. With homogeneous films, $\eta^*/\eta_{wat} \sim 10^2$ would have been enough to guarantee Sauerbrey behavior. In other words, effects of viscoelasticity are more pronounced for adsorbed spheres than for homogeneous films. In the case of homogeneous films, the contribution of the film's finite viscosity to the frequency shift is given by the second term in parentheses in eq 2:

$$\frac{\Delta f^*}{f_F} \approx \frac{-\omega m_f}{\pi Z_q}\left(1 - \frac{Z_{liq}^2}{Z_f^2}\right) = \frac{-\omega m_f}{\pi Z_q}\left(1 - \frac{\eta_{liq}}{\eta_f}\frac{\rho_{liq}}{\rho_f}\right) \qquad (2)$$

The indices f and liq denote the film and the liquid, respectively. m_f is the mass per unit area of the film. As eq 2 shows, viscoelasticity affects the frequency shift at a level of (let us say) 1%, if the viscosity of the film is 100 times the viscosity of the liquid. For spheres, on the other hand, viscoelastic effects are still very appreciable at $\eta^*/\eta_{wat} = 10^2$ (deviation of Δf from the value at infinite stiffness still is ~20%; see Figure 8a). Clearly, there is a qualitative difference between the two geometries. The difference goes back to the strong concentration of stress close to the contact line (Figure 9). Due to the peak in stress at the rim of the contact, even rather stiff objects move relative to the crystal surface if the latter oscillates. The detailed analysis shows that the movement of the sphere mostly amounts to a rocking of the entire sphere. More, specifically, the vorticity of the velocity is almost constant inside the spheres, as it should be for a pure rotation. The bulk of the sphere remains essentially undeformed. Only the contact zone undergoes oscillatory deformation.

We conclude with remarks on "apparent softness". The overtone dependence that was observed experimentally and in

(44) Hinrichsen, E. L.; Feder, J.; Jossang, T. *Phys. Rev. A* **1990**, *41*, 4199. (a) The fractional volume of the adsorbate in a film of height $2R$ (R the radius of the spheres) is $\varphi = \theta V_{sphere}/V_{projected}$, where $V_{sphere} = 4\pi/3R^3$ is the sphere volume and $V_{projected} = 2pR^3$ is the projected area of a sphere times its height. Inserting numbers, one finds $\varphi = 0.37$. The fractional amount of trapped solvent is equal to $(1-\varphi)/\varphi$, which is 1.73.

(45) Macakova, L; Blomberg, E; Claesson, P. M. *Langmuir* **2007**, *23*, 12436.

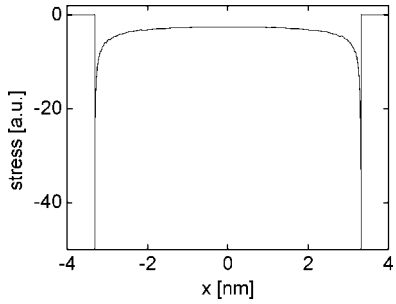

Figure 9. Local tangential stress onto the left-hand side wall of the simulation cell as shown in Figure 3a. The stress peaks at the three-phase lines.

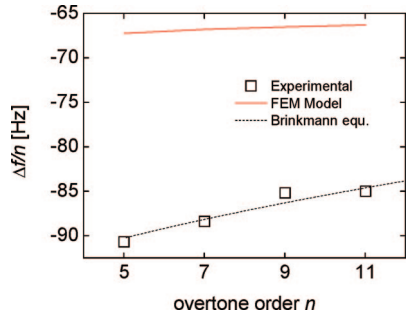

Figure 10. Normalized frequency shift, $\Delta f/n$, versus overtone order, n. The coverage in this particular case was 40%. The model assumed perpendicular flow for the truncated sphere. The dashed line was calculated with eq 4, assuming a thickness of $L = 38$ nm and a permeability of $\xi = 21$ nm. The magnitude of $\Delta f/n$ decreases for all data sets. For planar layers, such an overtone dependence of the apparent Sauerbrey mass would be interpreted as an indication of softness. In the case of the FEM model and the Brinkman-based model, it is of entirely hydrodynamic origin.

the simulations (Figure 10) has negative sign ($|\Delta f|$ decreases with increasing overtone order). Such a behavior would typically be associated with finite softness. This can be understood by revisiting eq 2:

$$\frac{\Delta f^*}{f_F} \approx \frac{-\omega m_f}{\pi Z_q}\left(1 - \frac{\eta_{liq}}{\eta_f}\frac{\rho_{liq}}{\rho_f}\right) = \frac{-\omega m_f}{\pi Z_q}\left(1 - \frac{i\omega\eta_{liq}}{G_f}\frac{\rho_{liq}}{\rho_f}\right)$$

$$\frac{\Delta f}{n} \approx \frac{-2\pi n f_F^2 m_f}{\pi Z_q}\left(1 - J_f'' 2\pi n f_F \eta_{liq}\frac{\rho_{liq}}{\rho_f}\right) \quad (3)$$

Here $J_f = 1/G_f = 1/(i\omega\eta_f)$ is the film's viscoelastic compliance. The more compliant the film is, the larger is the overtone dependence of $\Delta f/n$. Note that J_f'' itself also depends on frequency, which implies a second, implicit dependence of $\Delta f/n$ on n, in addition to the explicit one.

As discussed above, in FEM modeling, the spheres were modeled as rigid. For the simulation, therefore, the overtone dependence cannot be a consequence of softness, it must be of hydrodynamic origin. To further substantiate this statement, we compare our data with the results of an effective medium theory of rough surfaces as provided in ref 26. These authors treat roughness with the Brinkman equation. This equation describes flow in porous media. Therefore, the rough surface is treated as a film of thickness L with permeability ξ. The thickness of the film, L, is the vertical scale of roughness. The interpretation of the permeability, ξ, for a rough surface is not entirely clear. Therefore, at this point, we do not discuss the interpretation of this parameter, focusing on the ability of the Brinkman model to reproduce the overtone dependence of the normalized frequency shift. Evaluating the stress at the bottom of this "film" and applying the small-load approximation, one finds

$$\frac{\Delta f^*}{f_F} \approx \frac{i}{\pi Z_q}\sqrt{i\omega\rho\eta} - \frac{\omega\rho d_{eff}^*}{\pi Z_q}$$
$$d_{eff}{}^* = \frac{L}{\xi_H^2 q_1^2} - \frac{1}{W}\frac{1}{\xi_H^2 q_1^2}\left\{\frac{2q_0}{q_1}[\cosh(q_1 L) - 1] + \sinh(q_1 L)\right\}$$
$$q_0 = \sqrt{\frac{i\omega\rho}{\eta}} = \frac{1+i}{\delta}$$
$$q_1^2 = q_0^2 + \xi_H^{-2},$$
$$W = q_1\cosh(q_1 L) + q_0\sinh(q_1 L) \quad (4)$$

In the limit of $\xi_H \to 0$, the parameter $d_{eff}{}^*$ is equal to L and the layer looks like to Sauerbrey film. Provided that the free parameters are chosen suitably, the Brinkman film reproduces the experimental results. Figure 10 shows a comparison. The coverage was 40%, $L = 38$ and $\xi_H = 21$ nm, respectively, were chosen to give reasonable agreement with the experimental data. Indeed, the Brinkman model predicts a decrease of $|\Delta f/n|$ with overtone order, although the film is rigid. This overtone dependence must be caused by hydrodynamics. This finding corroborates our statement that hydrodynamics induces an overtone dependence of the Sauerbrey mass, which might be misinterpreted as a consequence of softness.

The overtone dependence observed in the experiment is stronger than that predicted by the FEM calculations. In part, this is a consequence of a finite compliance of the protein molecules. Just as the parameters derived from fitting QCM data with the effective media models (eq 2) will contain hydrodynamic contribution, those derived from the application of the Brinkman model will contain a contribution from the elastic properties of the adsorbed materials. In both cases, the physical meaning of the respective model parameters is vague. As a side remark, the presence of protein aggregates also induces an overtone dependence, which was shown to have a hydrodynamic origin as well.[39] Despite the extensive purification procedures employed, the presence of some aggregates is unavoidable, especially in the case of experiments aimed at obtaining high surface coverage.

Summarizing the remarks on softness, adsorbed spheres appear softer than corresponding films of the same material for two reasons. First, the spheres may rock back and forth. At large amplitude, the rocking motion would turn into rolling. Clearly, this displacement pattern is impossible for films. Second, the flow of solvent around the spheres generates an apparent softness, even if the spheres are perfectly rigid.

CONCLUSIONS

We find good agreement between experimental results on frequency versus coverage for adsorbed ferritin, on one hand, and the corresponding FEM model, on the other. Since there is little choice in the input parameters to the FEM calculation, the model is predictive. In acoustic terms, the adsorbate looks like a Sauerbrey film even at coverages much below 50%. The relation

between coverage and frequency shift is nonlinear in the sense that Δf levels off at high coverage because of the trapped solvent. At low coverage, the volume of the trapped solvent is about three times as large as the volume of the adsorbate. Softness has a stronger effect for adsorbed spheres compared to continuous films because the spheres may rock back and forth on the resonator surface. Also, there is a hydrodynamic effect leading to an apparent softness (that is, a dependence of the Sauerbrey mass on the overtone order).

APPENDIX

Small-Load Approximation in Tensor Form. In the main text, the load impedance is treated as a scalar quantity. It is the ratio of shear stress (in the $x-z$ plane) to the velocity of the crystal surface, which is along x. Technically, one might view Z_L as the xzx-component of the third rank tensor defined as

$$\sigma_{ij} = Z_{L,ijkl}\omega u_k \tag{5}$$

Clearly, there are stress components other than the xz-component if the sample is of some complex nature. For the geometry given here, one can argue that all components other than the xz-component would average out on the macroscopic scale for reasons of symmetry. Still, the question is of broad relevance, and we take the opportunity to formulate the small-load approximation in a more general form. The result of this calculation applies to resonators of arbitrarily complex shape and arbitrary samples.

Consider the unloaded resonator first. Is characterized by a density distribution $\rho(r)$ and a stiffness tensor $c_{ijkl}(r)$. Let the displacement field be $u_k(r)$. A resonant mode is the solution to the eigenvalue problem

$$\frac{1}{\rho}\nabla \cdot c : (\nabla \otimes u) = -\omega^2 u \tag{6}$$

Here "$\cdot$" and ":" denote contraction and double contraction, respectively. $\otimes$ is the outer product. In coordinate form, $\nabla\otimes u$ is given as $\partial u_k/\partial x_l$. $-\omega^2$ is the eigenvalue and u is the eigenfunction. The left-hand side could be also written as $\hat{D}u$ with $\hat{D} = 1/\rho\ (\nabla\cdot c:\nabla\otimes...)$ an operator.

Now let there be a load at the surface of the resonator. The corresponding eigenvalue problem reads as

$$\frac{1}{\rho}\nabla \cdot c : (\nabla \otimes u) - \delta(r-S)\frac{1}{\rho}\hat{n}\cdot \mathrm{i}\omega Z_L \cdot u = -(\omega^2 + \Delta(\omega^2))u \tag{7}$$

The second term on the left-hand side describes the acceleration induced by the load at the surface, S. $\delta(r-S)$ is the Dirac δ function. The second term only applies to locations at the surface. The stress exerted by the sample is $\mathrm{i}\omega Z_L\cdot u$. Again, Z_L now is third-rank tensor. The stress is transported along the surface normal, $\hat{n}$. The minus sign enters because the stress is exerted onto the crystal by the sample. The term $1/\rho\ \hat{n}\cdot \mathrm{i}\omega Z_L(\omega)\cdot u$ therefore is an acceleration, as is the right-hand side. $\Delta\omega^2 = 2\omega\Delta\omega$ is the shift of the eigenvalue induced by the perturbation, where the perturbation is the small load. $\Delta\omega^2$ can be straightforwardly calculated by perturbation theory. The formalism is well-known from quantum mechanics, where the operator typically is the Hamiltonian. It is readily adapted to partial differential operators, as shown below.

Subtraction of eq 6 from eq 7 yields

$$\delta(r-S)\frac{1}{\rho}\hat{n}\cdot \mathrm{i}\omega Z_L \cdot u = -\Delta(\omega^2)u = 2\omega\Delta\omega u \tag{8}$$

As in quantum mechanics, we multiply with u from the left and integrate over the volume:

$$\int_V \delta(r-S)\frac{1}{\rho}u\cdot\hat{n}\cdot \mathrm{i}\omega Z_L\cdot u\ \mathrm{d}V = 2\omega\Delta\omega u\int_V u\cdot u\ \mathrm{d}V \tag{9}$$

We normalize the displacement field, $\int_V u\cdot u\ \mathrm{d}V$ evaluates to unity. Also making use of the Dirac δ, we find

$$\Delta f = \frac{\Delta\omega}{2\pi} = \frac{\mathrm{i}}{4\pi}\int_S \frac{1}{\rho}u\cdot\hat{n}\cdot Z_L\cdot u\ \mathrm{d}S \tag{10}$$

Equation 10 is the small-load approximation in tensor form.

In the following, we show that eq 10 reduces to eq 1 for thickness shear resonators. In this case, the displacement field has only one component ($u_x(z)$), given by

$$u_x(z) = \frac{1}{N}\sin\left(\frac{\pi z}{d_q}\right) \tag{11}$$

Here d_q is the thickness of the crystal and N is a normalization constant. The origin of the z-scale is in the center of the crystal. Requiring $\int_V u\cdot u\ \mathrm{d}V = 1$ leads to

$$u_x(z) = \sqrt{\frac{2}{A_q d_q}}\sin\left(\frac{\pi z}{d_q}\right) \tag{12}$$

Here A_q is the area of the crystal. Inserting this result into eq 10 yields

$$\begin{aligned}\Delta f &= \frac{\mathrm{i}}{4\pi}\frac{2}{\rho A_q d_q}\int_S \hat{x}\cdot\hat{z}\cdot Z_L\cdot\hat{x}\ \mathrm{d}S \\ &= \frac{\mathrm{i}}{4\pi}\frac{2}{\rho A_q d_q}A_q Z_{L,xzx} \\ &= \frac{\mathrm{i}}{\pi}\frac{f_F}{Z_q}Z_{L,xzx}\end{aligned} \tag{13}$$

$\hat{x}$ and $\hat{z}$ are unit vectors. Since $Z_{L,xzx}$ is laterally homogeneous, the integration over the surface yields the area of the surface as a prefactor. The last transformation made use of the relation

$$\rho d_q = \rho\frac{\lambda}{2} = \frac{\rho v_q}{2f_F} = \frac{Z_q}{2f_F} \tag{14}$$

Here λ is the wavelength of transverse sound, v_q is the speed of sound, and $Z_q = \rho v_q$ is the acoustic impedance. Identifying Z_L from eq 1 with $Z_{L,xzx}$ from eq 13, one sees that the small-load approximation in tensor reduces to eq 1. Further, eq 13 shows that only shear stress in the xz-plane contributes to the frequency shift.

Again, the significance of eq 10 goes much beyond the proof that only shear stress matters in the calculation of Δf for the conventional QCM. It can be used to calculate the complex frequency shift of any acoustic resonator (including, for instance, microcantilevers,[46] wine glass resonators,[47] and suspended bars[48]) from the stress/speed ratio (in its tensor form) at the resonator surface.

Even for the standard QCM, the tensor form of the small-load approximation allows a statement on two familiar problems, which are roughness and flexural modes. Suppose that the surface normal at some location does not point along z, but rather has components (n_x,n_x,n_z), where $n_x^2 + n_y^2 + n_z^2 = 1$. Let the displacement be entirely along x. Equation 10 then reads

$$\begin{aligned}\Delta f &= \frac{\mathrm{i}}{4\pi}\int_S u_x^2 \frac{1}{\rho}(n_x Z_{\mathrm{L},xxx} + n_y Z_{\mathrm{L},xyx} + n_z Z_{\mathrm{L},xzx})\ \mathrm{d}S \\ &= \frac{\mathrm{i}}{4\pi}\int_S u_x^2 \frac{1}{\rho}\left(n_x \frac{\sigma_{xx}}{u_x} + n_y \frac{\sigma_{yx}}{u_x} + n_z \frac{\sigma_{zx}}{u_x}\right)\mathrm{d}S \\ &= \frac{\mathrm{i}}{4\pi}\int_S u_x \frac{1}{\rho}(n_x\sigma_{xx} + n_y\sigma_{yx} + n_z\sigma_{zx})\ \mathrm{d}S\end{aligned} \tag{15}$$

Considering flexural constributions, suppose that the surface is perfectly flat, but that the displacement has some vertical component, u_z, due to bending. The displacement pattern still is normalized such that such that $\int_V \boldsymbol{u}\cdot\boldsymbol{u}\ \mathrm{d}V = \int_V u_x^2 + u_z^2\ \mathrm{d}V = 1$. Equation 10 then reads

$$\begin{aligned}\Delta f &= \frac{\mathrm{i}}{4\pi}\int_S \frac{1}{\rho}\left(u_x^2\frac{\sigma_{xz}}{u_x} + u_z^2\frac{\sigma_{zz}}{u_z} + u_z u_x\left(\frac{\sigma_{xz}}{u_z} + \frac{\sigma_{zz}}{u_x}\right)\right)\mathrm{d}S \\ &= \frac{\mathrm{i}}{4\pi}\int_S \frac{2}{\rho}(u_x\sigma_{xz} + u_z\sigma_{zz})\ \mathrm{d}S\end{aligned} \tag{16}$$

Of course, the mixed case (a rough crystal surface undergoing both tangential and normal displacements) can also be treated by eq 10. We stop providing explicit equations here.

ACKNOWLEDGMENT

I.R. was the recipient of the Alexander von Humboldt Foundation research fellowship. He acknowledges the Department of Industry of the Basque Country for the generous start-up funding. We thank Markus Herrscher for stimulating discussions and Uwe Cronjäger for making the QCM-AFM cell.

SUPPORTING INFORMATION AVAILABLE

Additional information as noted in text. This material is available free of charge via the Internet at http://pubs.acs.org.

Received for review June 26, 2008. Accepted September 8, 2008.

AC8013115

(46) Rabe, U.; Janser, K.; Arnold, W. *Rev. Sci. Instrum.* **1996**, *67*, 3281.

(47) Xie, Y.; Li, S. S.; Lin, Y. W.; Ren, Z. Y.; Nguyen, C. T. C. *IEEE Trans. Ultrasonics Ferroelectr. Frequency Control* **2008**, *55*, 890.

(48) Ekinci, K. L.; Roukes, M. L. *Rev. Sci. Instrum.* **2005**, *76*, 061101.

(49) Edvardsson, M.; Rodahl, M.; Kasemo, B.; Hook, F. *Anal. Chem.* **2005**, *77*, 4918.

(50) Domack, A.; Prucker, O.; Rühe, J.; Johannsmann, D. *Phys. Rev. E* **1997**, *56*, 680.